Hollow Mesoporous Fe_2O_3 Nanospindles/CNTs Composite: An Efficient Catalyst for High-Performance $Li-O_2$ Batteries

Hairong Xue[1], Yiou Ma[1], Tao Wang[1]*, Hao Gong[1], Bin Gao[1], Xiaoli Fan[1], Juanjuan Yan[1], Xianguang Meng[2], Songtao Zhang[3] and Jianping He[1]*

[1] Jiangsu Key Laboratory of Materials and Technology for Energy Conversion, College of Materials Science and Technology, Nanjing University of Aeronautics and Astronautics, Nanjing, China, [2] Photofunctional Materials Research Platform, College of Materials Science and Engineering, North China University of Science and Technology, Tangshan, China, [3] Testing Center, Yangzhou University, Yangzhou, China

The design of mesoporous or hollow transition metal oxide/carbon hybrid catalysts is very important for rechargeable $Li-O_2$ batteries. Here, spindle-like Fe_2O_3 with hollow mesoporous structure on CNTs backbones (Fe_2O_3-HMNS@CNT) are prepared by a facile hydrolysis process combined with low temperature calcination. Within this hybrid structure, the hollow interior and mesoporous shell of the Fe_2O_3 nanospindles provide high specific surface area and abundant catalytical active sites, which is also beneficial to facilitating the electrolyte infiltration and oxygen diffusion. Furthermore, the crisscrossed CNTs form a three-dimensional (3D) conductive network to accelerate and stabilize the electron transport, which leads to the decreasing internal resistance of electrode. As a cathodic catalyst for $Li-O_2$ batteries, the Fe_2O_3-HMNS@CNT composite exhibits high specific capacity and excellent cycling stability (more than 100 cycles).

Keywords: hollow mesoporous structure, carbon support, transition metal oxides, cathodic catalyst, $Li-O_2$ batteries

INTRODUCTION

To meet the global energy demand, the development of the clean and sustainable energy storage or conversion devices is very important (Tarascon and Armand, 2011; Lu et al., 2014; Wang et al., 2017; Zhang et al., 2018; Gao et al., 2019). Rechargeable $Li-O_2$ battery has attracted wide attention as a new energy storage device, due to its high theoretical energy density ($\sim$3,500 Wh kg^{-1}) (Tarascon and Armand, 2011; Lu et al., 2014). However, the practical application of $Li-O_2$ batteries still suffer a series of problems, including high overpotentials, low rate capacity and poor cycle stability, which primarily originates from its sluggish kinetics for oxygen reduction reaction (ORR) and oxygen evolution reaction (OER) (Bruce et al., 2012; Wang et al., 2014). At the cathode (air electrode), the gradual formation of the insoluble discharge products Li_2O_2 may block the inward oxygen diffusion of and electrolyte infiltration, which results in the rapid decline of battery performance (Zhao et al., 2015; Wang et al., 2016). To overcome these challenges, the design and development of the high-performance catalysts for oxygen-involved reactions are highly desired for the $Li-O_2$ batteries.

In recent years, a lot of the efforts have been devoted to investigate the highly active and stable catalysts for the $Li-O_2$ batteries, such as carbons, precious metals, and transition metal oxides. As the common catalysts, the inexpensive carbon materials have high surface area, nevertheless, their

limited catalytic activity for both OER and ORR restricts the battery performance of the Li-O$_2$ batteries (Girishkumar et al., 2010; Shui et al., 2013). Since the nanoporous gold (NPG) was used as a cathode catalyst, various precious metals (e.g., Ru, RuO, and Pd) have been adopted in the Li-O$_2$ batteries (Peng et al., 2012; Lu et al., 2013; Ottakam Thotiyl et al., 2013; Li et al., 2014, 2015). Although the cyclic stability can be distinctly enhanced by precious metal catalysts, the battery capacity is severely restricted because of the highly chemical formula weight. Moreover, high price of precious metals also hinders the large-scale commercialization in the Li-O$_2$ batteries. Benefiting from the low cost, high stability and good catalytic performance, transition metal oxides have been proposed as the promising catalysts for the Li-O$_2$ batteries (Wang H. et al., 2012; Chen et al., 2016; Gong et al., 2016, 2018a,b; Xue et al., 2016a,c; Dai et al., 2017; Tan et al., 2017; Feng et al., 2019). Many researches have indicated that Fe-based materials possess high catalytic activities for ORR in fuel cells and OER in water electrolysis (Bates et al., 2016; Song et al., 2019). Recently, some reports began to focus on iron oxides (Fe$_2$O$_3$), which can serve as the cathode catalyst in Li-O$_2$ batteries (Zhang et al., 2014). These works show the enhanced electrochemical performance (e.g., higher capacity and lower overpotentials) of the Li-O$_2$ batteries, however the cycling performance still needs to further improve. Therefore, it is necessary to explore an effective approach to enhance the catalytic performance of Fe$_2$O$_3$-based materials.

Tailoring of the morphology is an important method for obtaining the high-performance catalysts in various electrochemical application. Mesoporous hollow architectures show high surface area and large pore volume, which offers fast electron transfer paths and facilitates the electrolyte infiltration (Kresge et al., 1992; Inagaki et al., 2002; Malgras et al., 2016). Normally, mesoporous or hollow metallic oxide are prepared through the template-based methods, using either hard templates (e.g., carbon sphere and mesoporous silica) or soft templates (e.g., surfactants and polymer) (Attard et al., 1997; Crossland et al., 2013; Liu et al., 2015; Xue et al., 2016d). For these template methods, the multi-step processes are unavoidable, and the mesoporous of hollow structures may be damaged after removing the templates. Moreover, the resultant mesoporous or hollow frameworks often show poor crystalline degree and even amorphous, which limits their electrochemical performance (Lin et al., 2015). It should be noted that the low electronic conductivity is an intrinsic characteristic of the most metallic oxides. Although most of pure carbon materials possess low catalytic activity for OER and ORR, they are identified as the good catalyst support due to their high electric conductivity and large specific surface area (Hsin et al., 2007; Stein et al., 2009; Wu et al., 2009; Xia et al., 2018). Among various carbon materials, the carbon nanotubes (CNTs) show low density, very high strength, high chemical stability, and excellent conductivity (Sathiya et al., 2011; Wang Z. et al., 2012; Ma et al., 2018). These advantages are beneficial to fabricate hybrid or composite materials in many applications by using CNTs as useful substrates. However, the fabrication of mesoporous hollow Fe$_2$O$_3$ with high crystalline degree supported on CNTs by a simple and effective method is still an important challenge.

Inspired by the above idea, we proposed a Fe$_2$O$_3$/CNTs composite (denoted as Fe$_2$O$_3$-HMNS@CNT) prepared by using a simple hydrolysis reaction combined with heat treatment, in which spindle-like Fe$_2$O$_3$ with hollow mesoporous structure grown on CNTs backbones. Their hollow interior and mesoporous shell with high specific surface area offer abundant catalytical active sites for OER and ORR, which also promotes the diffusion and infiltration of electrolyte. Furthermore, a great deal of the crisscrossed CNTs form the three-dimensional (3D) conductive network, which benefits the fast and stable electron transport. As a cathodic catalyst for Li-O$_2$ batteries, the Fe$_2$O$_3$-HMNS@CNT exhibits good battery performance, especially excellent outstanding cycling stability (100 cycles).

EXPERIMENTAL METHODS

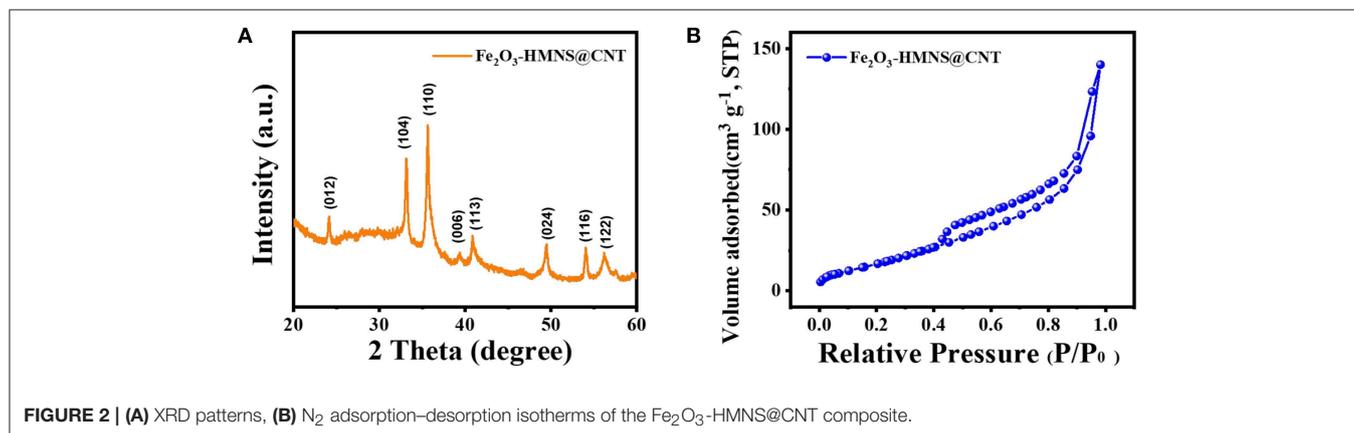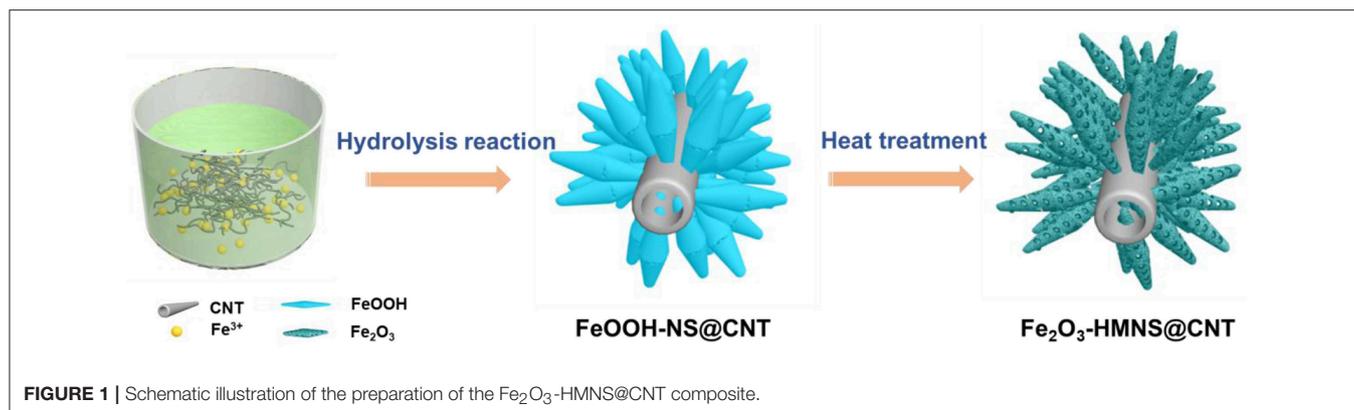### Hollow Mesoporous Fe$_2$O$_3$ Nanospindles on CNT Backbones

Carbon nanotubes (CNTs, 30–60 nm in diameter and 5–15 μm in length) were purchased from Shenzhen Nanotech Port Co. Ltd (Shenzhen, China). CNTs were refluxed in HNO$_3$ and then rinsed with distilled water. After drying, the obtained CNTs (10 mg) was dispersed in FeCl$_3$ solution (20 mL, 0.12 M) under sonication for 1 h. Then, the suspension was heated at 75°C for 6 h in an oil bath with stirring. After several rinsing combined with sonication, the products were dried at 60°C. Finally, the above products were annealed at 400°C for 4 h in air by using a slow heating rate (0.5°C min^{-1}) to form hollow mesoporous Fe$_2$O$_3$ nanospindles on CNT backbones.

Materials Characterization

The X-ray diffraction (XRD, Bruker D8 advance) with Cu Ka radiation ($\lambda = 1.5406$ Å) is used to analyze the crystal structure of the sample. The N$_2$ adsorption–desorption measurements conducted on a ASAP-2010 analyzer to investigate the pore structure. The Brunauer-Emmet-Teller (BET) method is used to calculate the specific surface area. The morphology and microstructure are observed by using field-emission scanning electron microscope (FE-SEM, Hitachi S-4800) and high-resolution transmission electron microscope (HR-TEM, JEOL JEM-2100), respectively.

Electrochemical Measurement

The electrochemical measurements are tested under two-electrode system at room temperature in the pure O$_2$ atmosphere, using Li plate as the counter and reference electrode. The work electrode is prepared by mixing Fe$_2$O$_3$-HMNS@CNT catalyst (50 wt %), Super P (45 wt %) and polytetrafluoroethylene (PTFE) binder (5 wt %), followed by vacuum drying at 100°C for 12 h. The capacity and current density of the sample is calculated by the whole electrode' weight. For the assembling of Li-O$_2$ battery, the working electrode and Li plate are separated by a glass-fiber separator in coin cell. The tetraethylene glycol dimethyl ether (TEGDME) containing lithium bis(tri-fluoromethane-sulfonyl)imide (LiTFSI) (1 M) is used as electrolyte. The Land 2100 Charge/Discharge instruments are carried to test the electrochemical measurements.

FIGURE 1 | Schematic illustration of the preparation of the Fe_2O_3-HMNS@CNT composite.

FIGURE 2 | (A) XRD patterns, **(B)** N_2 adsorption–desorption isotherms of the Fe_2O_3-HMNS@CNT composite.

RESULTS AND DISCUSSION

Figure 1 illustrates the fabrication of the mesoporous hollow Fe_2O_3 nanocrystals covered on CNT by a simple hydrolysis reaction combined with heat treatment. In order to facilitate the nucleation and anchoring of the nanocrystals on the CNT surface, these CNTs are functionally modified with carboxylic or hydroxyl groups under acidic reflux. During the subsequent stirring process, the electropositive Fe^{3+} ions can preferential adsorb the electronegative oxygen-containing groups on CNTs by the electrostatic attraction. Due to the hydrolysis of Fe^{3+} ions followed by the olation/oxolation of the FeO_6 units, the formed spindle-like β-FeOOH nanocrystals can be spontaneously grown on CNT backbones, which avoids the addition of any structure-directing agent. The TG/DSC is used to explore the reactions in the final annealing step (**Figure S1**). The TG curve show two mainly weight loss processes at 300°C and 300~400°C during the annealing step, which are attributed to the conversion from FeOOH into Fe_2O_3. The slowly intramolecular dehydration results in the slow weight loss before 300°C. After 300°C, a distinct weight loss can be found, which is originated from the fast removal of the H_2O molecules. After annealing treatment in air, the spindle-like β-FeOOH nanocrystals are converted to hollow mesoporous α-Fe_2O_3 nanospindles on CNT backbones (denoted as Fe_2O_3-HMNS@CNT) by the thermal dehydroxylation together with the lattice shrinkage.

The crystalline structure of the Fe_2O_3-HMNS@CNT composite is confirmed by XRD analysis. As shown in **Figure 2A**, the XRD pattern exhibits several intensively diffraction peaks at the 2θ values of about 24.2, 33.2, 35.6, 39.3, and 40.9°, which are indexed to the (012), (104), (110), (006), and (113) facets of the hexagonal α-Fe_2O_3. This result of XRD is in accord with the standard card of α-Fe_2O_3 (JCPDS no. 33-0664). The pore structure of the Fe_2O_3-HMNS@CNT composite is analyzed by N_2 adsorption–desorption isotherms (**Figure 2B**). It can be seen that there is a type-IV curve of the Fe_2O_3-HMNS@CNT with a distinctly hysteresis loop on N_2 adsorption–desorption isotherms, which indicates the typically mesoporous structure (Deng et al., 2007; Xue et al., 2016b). Moreover, the nitrogen uptake is found from 0.40 to 0.70 (P/P_o), which can be attributed to the mesoporous materials' capillary condensation of nitrogen. Based on N_2 adsorption–desorption isotherms, the specific surface area is calculated to be 97 m^2 g^{-1}. The above results indicate that the Fe_2O_3-HMNS@CNT has a typically mesoporous structure with high specific surface area.

The morphologies and structures of the Fe_2O_3-HMNS@CNT composite are observed by scanning electron microscopy (SEM) and transmission electron microscopy (TEM). As shown in **Figure S2**, the CNT shows the typical one-dimensional tubular structure with a diameter of ~40 nm. **Figure 3a** reveals a panoramic view of the sample, in which the spindle-like nanocrystals grown on the entire surface of the sinuous CNTs

backbones. It can be noted that there are many obvious porous within the Fe_2O_3 nanospindles, as shown in **Figures 3b,c**. TEM observation is used to further investigate the internal structure of the sample. The spindle-like Fe_2O_3 nanocrystals have a diameter of around 80 nm and a length of about 250 nm (**Figure 3d**), which show a well-developed hollow interior (marked by orange dotted line) and a typically mesoporous shell (marked by purple dotted line) (**Figure 3e**). During the calcining process, the

decomposition-oxidation of the FeOOH can release abundant H_2O and gases, which leads to the formation of mesoporous structure. On the other hand, the density of FeOOH (3 g cm^{-3}) is lower than that of the hematite (Fe_2O_3, 5.3 g cm^{-3}), so some internal mesoporous slowly forms the larger porous to maintain the spindle-like structure during the lattice shrinkage process, thus leading to the formation of the hollow interior together with the mesoporous shell. As shown in **Figure 3f**, some clear lattice
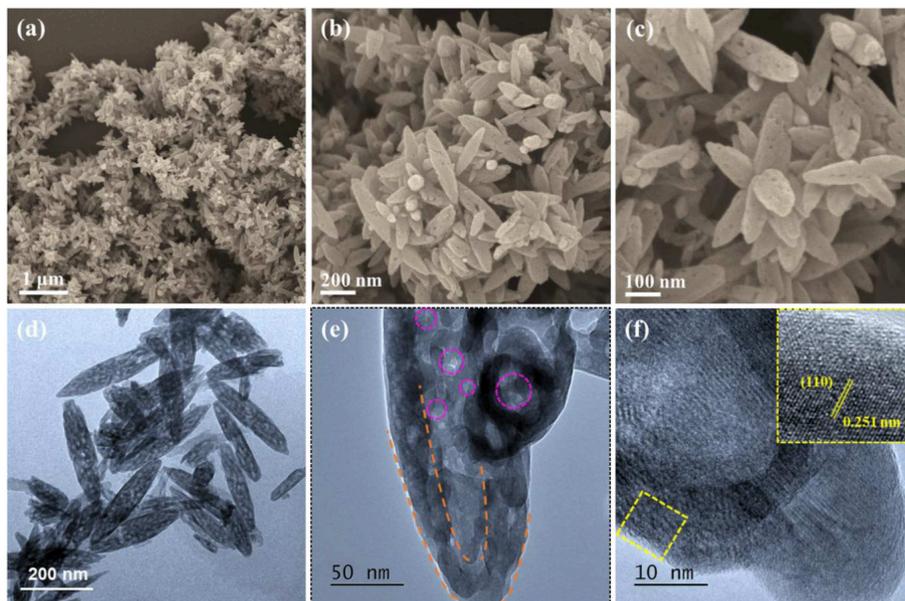

FIGURE 3 | **(a–c)** FESEM, **(d–f)** HRTEM images of the Fe_2O_3-HMNS@CNT composite.
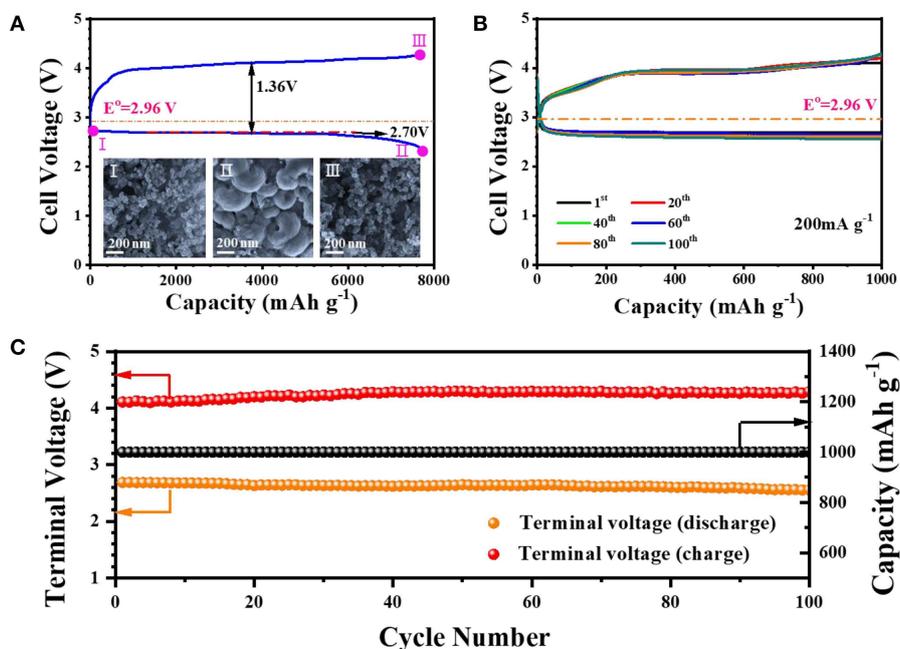

FIGURE 4 | **(A)** The fully discharging and charging curves in the first cycle and the SEM images [inset of **(A)**], **(B)** cyclic stability tested under a limited capacity (1,000 mAh g^{-1}), and **(C)** the variation of the terminal charge/discharge voltages and specific capacity over 100 cycles of the Fe_2O_3-HMNS@CNT-based cathode.

fringes with an interplanar spacing of 0.251 nm in a single Fe_2O_3 nanospindle, corresponding to the (110) planes of the hexagonal α-Fe_2O_3, which confirms the formation of the α-Fe_2O_3 with high crystallinity.

Inspired by the superiorities of material and structure, the Fe_2O_3-HMNS@CNT composite is investigated as the cathodic catalyst for rechargeable Li-O_2 batteries. **Figure 4A** shows the discharge and charge curves of the sample, which is tested under O_2 atmosphere with a current density of 200 mA g^{-1}. The Fe_2O_3-HMNS@CNT-based cathode exhibits a large discharge capacity of 7,730 mAh g^{-1} and a high discharge plateau ($\sim$2.70 V) with the low overpotential for discharging (0.26 V). Owing to the low overpotential (1.10 V) for the charge process, the coulombic efficiency of the sample is closed to 100%. The reversible formation/decomposition of the discharging product Li_2O_2 can be confirmed by SEM (inset of **Figure 4A**). After fully discharging (defined as II), it is seen that a mass of the Li_2O_2 particles with the typically toroid-like shape uniformly cover on the electrode surface, which is observably different from the fresh electrode (defined as I). When the electrode is fully charged, the formed Li_2O_2 particles is rarely observed (defined as III), indicating high reversibility of the Fe_2O_3-HMNS@CNT-based cathode. We further evaluate the cycling performance of the Fe_2O_3-HMNS@CNT-based cathode, tesed under the limited capacity (1,000 mAh g^{-1}). It can be found that the sample has the small discharge and charge overpotentials of 0.24 and 0.93 V in the first cycle, respectively, which implies the high catalytic activity for both OER and ORR (**Figure 4B**). After 100 cycles, no distinct change of the specific capacities of the sample is observed in discharging/charging curves. Moreover, the discharging and charging terminal voltages can still maintain in 2.6 and 4.3 V. These results exhibit the excellent cycling stability of the Fe_2O_3-HMNS@CNT-based cathode (**Figure 4C**). As a reference, the cycling stability of the Fe_2O_3-HMNS@CNT-based cathode is much better than those of previously reported non-precious metal/metal oxide-based materials (**Table S1**).

As the cathodic catalyst for rechargeable Li-O_2 batteries, the as-prepared Fe_2O_3-HMNS@CNT composite exhibits the excellent cycling stability, which not only benefits by the intrinsic material characteristics but also dependents on the morphology and structure. On the one hand, these largely separated Fe_2O_3 nanospindles directly grown on the CNT backbones, which makes them accessible to the electrolyte. Different from the conventional nanoparticle catalysts, the adverse agglomeration of the Fe_2O_3-HMNS@CNT can be effectively decreased, avoiding the elimination of the active interfaces. The Fe_2O_3 with a hollow interior and a mesoporous shell offers high specific surface area and a mass of catalytical active sites, which also facilitates the diffusion and infiltration of electrolyte. On the other hand, the 3D conductive network composed of the crisscrossed CNTs ensures

the fast and stable electron transport, leading to the lower internal resistance of electrode.

CONCLUSION

In summary, we successfully fabricated hollow mesoporous Fe_2O_3 nanospindles on CNTs (Fe_2O_3-HMNS@CNT) though a simple hydrolysis reaction followed by a heat treatment, which are served as cathodic catalyst for Li-O_2 batteries. In this catalyst design concept, the spindle-like Fe_2O_3 nanocrystals possess the hollow interior and mesoporous shell, which not only provides high specific surface area and abundant catalytical active sites but also facilitates the diffusion and infiltration of electrolyte. Moreover, the 3D conductive network formed by the crisscrossed CNTs ensures the fast and stable electron transport, reducing internal resistance of electrode. Benefiting from the intrinsic material characteristics and structural superiorities, the Fe_2O_3-HMNS@CNT catalyst shows high specific capacity and excellent cyclic stability.

DATA AVAILABILITY

All datasets generated for this study are included in the manuscript/**Supplementary Files**.

AUTHOR CONTRIBUTIONS

HX, TW, and JH conceived this research work. HX performed the experiments and wrote the manuscript. YM, HX, HG, BG, XF, and JY tested the electrochemical performance. XM and SZ contributed to analyze the experimental results. All authors read and approved the final manuscript.

FUNDING

SUPPLEMENTARY MATERIAL

The Supplementary Material for this article can be found online at: https://www.frontiersin.org/articles/10.3389/fchem.2019.00511/full#supplementary-material

REFERENCES

Attard, G., Bartlett, P., Coleman, N., Elliott, J., Owen, J., and Wang, J. (1997). Mesoporous platinum films from lyotropic liquid crystalline phases. *Science*. 278, 838–840. doi: 10.1126/science.278.5339.838

Bates, M., Jia, Q., Doan, H., Liang, W., and Mukerjee, S. (2016). Charge-transfer effects in Ni-Fe and Ni-Fe-Co mixed-metal oxides for the alkaline oxygen evolution reaction. *ACS Catal.* 6, 155–161. doi: 10.1021/acscatal.5b01481

Bruce, P. G., Freunberger, S. A., Hardwick, L. J., and Tarascon, J. M. (2012). Li-O2 and Li-S batteries with high energy storage. *Nat. Mater.* 11, 19–29. doi: 10.1038/nmat3191

Chen, Y., Pang, W. K., Bai, H., Zhou, T., Liu, Y., Li, S., et al. (2016). Enhanced structural stability of nickel-cobalt hydroxide via intrinsic pillar effect of metaborate for high-power and long-life supercapacitor electrodes. *Nano Lett.* 17, 429–436. doi: 10.1021/acs.nanolett.6b04427

Crossland, E. J., Noel, N., Sivaram, V., Leijtens, T., Alexander-Webber, J. A., and Snaith, H. J. (2013). Mesoporous TiO2 single crystals delivering enhanced mobility and optoelectronic device performance. *Nature* 495, 215–219. doi: 10.1038/nature11936

Dai, Z., Geng, H., Wang, J., Luo, Y., Li, B., Zong, Y., et al. (2017). Hexagonal-phase cobalt monophosphosulfide for highly efficient overall water splitting. *ACS. Nano* 11, 11031–11040. doi: 10.1021/acsnano.7b05050

Deng, Y., Liu, C., Yu, T., Liu, F., Zhang, F., Wan, Y., et al. (2007). Facile synthesis of hierarchically porous carbons from dual colloidal crystal/block copolymer template approach. *Chem. Mater.* 19, 3271–3277. doi: 10.1021/cm070600y

Feng, Y., Xue, H., Wang, T., Gong, H., Gao, B., Xia, W., et al. (2019). Enhanced Li2O2 decomposition in rechargeable Li-O2 battery by incorporating WO3 nanowire array photocatalyst. *ACS Sustain. Chem. Eng.* 7, 5931–5939. doi: 10.1021/acssuschemeng.8b05944

Gao, B., Wang, T., Fan, X., Gong, H., Li, P., Feng, Y., et al. (2019). Enhanced water oxidation reaction kinetics on a BiVO4 photoanode by surface modification with Ni4O4 cubane. *J. Mater. Chem. A* 7, 278–288. doi: 10.1039/C8TA09404G

Girishkumar, G., McCloskey, B., Luntz, A., Swanson, S., and Wilcke, W. (2010). Lithium-air battery: promise and challenges. *J. Phys. Chem. Lett.* 1, 2193–2203. doi: 10.1021/jz1005384

Gong, H., Wang, T., Guo, H., Fan, X., Liu, X., Song, L., et al. (2018a). Fabrication of perovskite-based porous nanotubes as efficient bifunctional catalyst and application in hybrid lithium-oxygen batteries. *J. Mater. Chem. A* 6, 16943–16949. doi: 10.1039/C8TA04599B

Gong, H., Wang, T., Xue, H., Fan, X., Gao, B., Zhang, H., et al. (2018b). Photo-enhanced lithium oxygen batteries with defective titanium oxide as both photo-anode and air electrode. *Energy Storage Mater.* 13, 49–56. doi: 10.1016/j.ensm.2017.12.025

Gong, H., Xue, H., Wang, T., Guo, H., Fan, X., Song, L., et al. (2016). High-loading nickel cobaltate nanoparticles anchored on three-dimensional N-doped graphene as an efficient bifunctional catalyst for lithium-oxygen batteries. *ACS Appl. Mater. Interfaces* 8, 18060–18068. doi: 10.1021/acsami.6b04810

Hsin, Y. L., Hwang, K. C., and Yeh, C. T. (2007). Poly (vinylpyrrolidone)–modified graphite carbon nanofibers as promising supports for PtRu catalysts in direct methanol fuel cells. *J. Am. Chem. Soc.* 129, 9999–10010. doi: 10.1021/ja072367a

Inagaki, S., Guan, S., Ohsuna, T., and Terasaki, O. (2002). An ordered mesoporous organosilica hybrid material with a crystal-like wall structure. *Nature* 416, 304–307. doi: 10.1038/416304a

Kresge, C., Leonowicz, M., Roth, W., Vartuli, J., and Beck, J. (1992). Ordered mesoporous molecular sieves synthesized by a liquid-crystal template mechanism. *Nature* 359, 710–712. doi: 10.1038/359710a0

Li, F., Tang, D., Jian, Z., Liu, D., Golberg, D., Yamada, A., et al. (2014). Li-O2 battery based on highly efficient Sb-doped Tin oxide supported Ru nanoparticles. *Adv. Mater.* 26, 4659–4664. doi: 10.1002/adma.201400162

Li, F., Tang, D., Zhang, T., Liao, K., He, P., Golberg, D., et al. (2015). Superior performance of a Li-O2 battery with metallic RuO2 hollow spheres as the carbon-free cathode. *Adv. Energy Mater.* 5:1500294. doi: 10.1002/aenm.201500294

Lin, J., Zhao, L., Heo, Y., Wang, L., Bijarbooneh, F., Mozer, A., et al. (2015). Mesoporous anatase single crystals for efficient Co(2+/3+)-based dye-sensitized solar cells. *Nano Energy* 11, 557–567. doi: 10.1016/j.nanoen.2014.11.017

Liu, J., Wickramaratne, N. P., Qiao, S. Z., and Jaroniec, M. (2015). Molecular-based design and emerging applications of nanoporous carbon spheres. *Nat. Mater.* 14, 763–774. doi: 10.1038/nmat4317

Lu, J., Lei, Y., Lau, K. C., Luo, X., Du, P., Wen, J., et al. (2013). Nanostructured cathode architecture for low charge overpotential in lithium-oxygen batteries. *Nat. Commun.* 4:2383. doi: 10.1038/ncomms3383

Lu, J., Li, L., Park, J., Sun, Y., Wu, F., and Amine, K. (2014). Aprotic and aqueous Li-O2 batteries. *Chem. Rev.* 114, 5611–5640. doi: 10.1021/cr400573b

Ma, L., Zhang, W., Wang, L., Hu, Y., Zhu, G., Wang, Y., et al. (2018). Strong capillarity, chemisorption, and electrocatalytic capability of crisscrossed nanostraws enabled flexible, high-rate, and long-cycling lithium-sulfur batteries. *ACS Nano* 12, 4868–4876. doi: 10.1021/acsnano.8b01763

Malgras, V., Ataee-Esfahani, H., Wang, H., Jiang, B., Li, C., Wu, K. C., et al. (2016). Nanoarchitectures for mesoporous metals. *Adv. Mater.* 28, 993–1010. doi: 10.1002/adma.201502593

Ottakam Thotiyl, M. M., Freunberger, S. A., Peng, Z., Chen, Y., Liu, Z., and Bruce, P. G. (2013). A stable cathode for the aprotic Li-O2 battery. *Nat. Mater.* 12, 1050–1056. doi: 10.1038/nmat3737

Peng, Z., Freunberger, S., Chen, Y., and Bruce, P. (2012). A reversible and higher-rate Li-O2 battery. *Science* 373, 563–566. doi: 10.1126/science.1223985

Sathiya, M., Prakash, A. S., Ramesha, K., Tarascon, J. M., and Shukla, A. K. (2011). V2O5-anchored carbon nanotubes for enhanced electrochemical energy storage. *J. Am. Chem. Soc.* 133, 16291–16299. doi: 10.1021/ja207285b

Shui, J. L., Okasinski, J. S., Kenesei, P., Dobbs, H. A., Zhao, D., Almer, J. D., et al. (2013). Reversibility of anodic lithium in rechargeable lithium-oxygen batteries. *Nat. Commun.* 4:2255. doi: 10.1038/ncomms3255

Song, L., Wang, T., Li, L., Wu, C., and He, J. (2019). [Fe(CN)6]2 derived Fe/Fe5C2@ N-doped carbon as a highly effective oxygen reduction reaction catalyst for zinc-air battery. *Appl. Catal. B Environ.* 244, 197–205. doi: 10.1016/j.apcatb.2018.11.005

Stein, A., Wang, Z., and Fierke, M. (2009). Functionalization of porous carbon materials with designed pore architecture. *Adv. Mater.* 21, 265–293. doi: 10.1002/adma.200801492

Tan, G., Chong, L., Amine, R., Lu, J., Liu, C., Yuan, Y., et al. (2017). Toward highly efficient electrocatalyst for Li-O2 batteries using biphasic N-doping cobalt@graphene multiple-capsule heterostructures. *Nano Lett.* 17, 2959–2966. doi: 10.1021/acs.nanolett.7b00207

Tarascon, J. M., and Armand, M. (2011). Issues and challenges facing rechargeable lithium batteries. *Nature* 414, 359–367. doi: 10.1038/35104644

Wang, H., Yang, Y., Liang, Y., Zheng, G., Li, Y., Cui, Y., et al. (2012). Rechargeable Li-O2 batteries with a covalently coupled MnCo2O4-graphene hybrid as an oxygen cathode catalyst. *Energy Environ. Sci.* 5, 7931–7935. doi: 10.1039/c2ee21746e

Wang, J., Zhang, Y., Guo, L., Wang, E., and Peng, Z. (2016). Identifying reactive sites and transport limitations of oxygen reactions in aprotic lithium-O2 batteries at the stage of sudden death. *Angew. Chem. Int. Ed.* 55, 5201–5205. doi: 10.1002/anie.201600793

Wang, X., Wang, Y., Bu, Y., Yan, X., Wang, J., Cai, P., et al. (2017). Influence of doping and excitation powers on optical thermometry in Yb3+-Er3+ doped CaWO4. *Sci. Rep.* 7:43383. doi: 10.1038/srep43383

Wang, Z., Luan, D., Madhavi, S., Hu, Y., and Lou, X. (2012). Assembling carbon-coated a-Fe2O3 hollow nanohorns on the CNT backbone for superior lithium storage capability. *Energy Environ. Sci.* 5, 5252–5256. doi: 10.1039/C1EE02831F

Wang, Z. L., Xu, D., Xu, J. J., and Zhang, X. B. (2014). Oxygen electrocatalysts in metal-air Batteries: from aqueous to nonaqueous electrolytes. *Chem. Soc. Rev.* 43, 7746–7786. doi: 10.1039/C3CS60248F

Wu, B., Hu, D., Kuang, Y., Liu, B., Zhang, X., and Chen, J. (2009). Functionalization of carbon nanotubes by an ionic-liquid polymer: dispersion of Pt and PtRu nanoparticles on carbon nanotubes and their electrocatalytic oxidation of methanol. *Angew. Chem. Int. Ed.* 48, 4751–4654. doi: 10.1002/anie.200900899

Xia, W., Li, J., Wang, T., Song, L., Guo, H., Gong, H., et al. (2018). The synergistic effect of Ceria and Co in N-doped leaf-like carbon nanosheets derived from a 2D MOF and their enhanced performance in the oxygen reduction reaction. *Chem. Commun.* 54, 1623–1626. doi: 10.1039/C7CC09212A

Xue, H., Mu, X., Tang, J., Fan, X., Gong, H., Wang, T., et al. (2016a). A nickel cobaltate nanoparticle-decorated hierarchical porous N-doped carbon nanofiber film as a binder-free self-supported cathode for non-aqueous Li-O2 batteries. *J. Mater. Chem. A* 4, 9106–9112. doi: 10.1039/C6TA01712F

Xue, H., Tang, J., Gong, H., Guo, H., Fan, X., Wang, T., et al. (2016b). Fabrication of PdCo bimetallic nanoparticles anchored on three-dimensional ordered N-doped porous carbon as an efficient catalyst for oxygen reduction reaction. *ACS Appl. Mater. Interfaces.* 8, 20766–20771. doi: 10.1021/acsami.6b05856

Xue, H., Wu, S., Tang, J., Gong, H., He, P., He, J., et al. (2016c). Hierarchical porous nickel cobaltate nanoneedle arrays as flexible carbon-protected cathodes for high-performance lithium-oxygen batteries. *ACS. Appl. Mater. Interfaces.* 8, 8427–8435. doi: 10.1021/acsami.5b10856

Xue, H., Zhao, J., Tang, J., Gong, H., He, P., Zhou, H., et al. (2016d). High-loading Nano-SnO2 encapsulated *in situ* in three-dimensional rigid porous

carbon for superior lithium-ion batteries. *Chem. Eur. J.* 22, 4915–4923. doi: 10.1002/chem.201504420

Zhang, T., Wang, Y., Song, T., Miyaoka, H., Shinzato, K., Miyaoka, H., et al. (2018). Ammonia, a switch for controlling high ionic conductivity in lithium borohydride ammoniates. *Joule* 2, 1522–1533. doi: 10.1016/j.joule.2018.04.015

Zhang, Z., Zhou, G., Chen, W., Lai, Y., and Li, J. (2014). Facile synthesis of Fe2O3 nanoflakes and their electrochemical properties for Li-air batteries. *ECS Electrochem. Lett.* 3, A8–A10. doi: 10.1149/2.006401eel

Zhao, C., Yu, C., Liu, S., Yang, J., Fan, X., Huang, H., et al. (2015). 3D porous N-doped graphene frameworks made of interconnected nanocages for ultrahigh-rate and long-life Li-O2 batteries. *Adv. Funct. Mater.* 25, 6913–6920. doi: 10.1002/adfm.201503077